

6

Structure and Stability of Aerated Food Emulsions

D. T. Wasan, W. Xu, A. Dutta, and A. Nikolov

Illinois Institute of Technology, Chicago, Illinois, U.S.A.

I. INTRODUCTION

The development of a stable structure and a suitable product texture in food emulsions and foam-based food products depends on the interactions between the fat globules and between fat globules and air bubbles (1). An important factor influencing the stability of food emulsions and foams is the developed fat particle structure. The fat particle structure variation and destabilization during the shearing process are very complex. Many factors such as shear rate, shear time, temperature, the composition of the surfactant mixture, and the ratio of liquid to solid content inside a fat globule can greatly affect the fat particle structure of the final product. Researchers have investigated some of these factors in relationship to emulsions.

Long-term stability of whipped foams is thought to result from the formation of a three-dimensional fat particle network structure (2,3). The presence of solid fat (to promote fat globule rupture) and of liquid fat (to promote clumping) might be necessary for the formation of a stable whipped foam. Darling (4) obtained similar results. He found that a prerequisite for effective whipping was that the solid part of the fat and the whipping time were directly related to the proportion of solid fat. Brooker and his colleagues (5,6) found that the development of a stable structure in a whipped foam depends on the interactions between the fat globules and between fat globules and air bubbles. The stabilization of air was a two-step process involving the selective adsorption of proteins and emulsions to the air-bubble surface, followed by the attachment of fat globules to the

air–water interface under shear stress. The attached globules stayed at the air–water interface in such a way that part of the fat became exposed to the air and slightly protruded into it. In the final product, bubbles were stabilized predominantly by the fat globules, but the remains of the initial protein-adsorbed interface persisted between the globules. In the aqueous phase, the fat particles form a three-dimensional network structure connecting different bubbles, which decreases the mobility of the bubbles and, hence, mechanically stabilizes the whipped product.

However, most information about the stability of whipped foams or foam-based products has come from studies utilizing simplified solutions that neglected the effect of the dispersed phase or from empirical studies providing information that was not easily translated quantitatively. The lack of detailed information from actual whipped foams stems from the lack of methods or tools to measure the component functional properties in systems as complex as whipped foams, which has prevented a further understanding of the relationship between component interactions (structure and conformation) and the stability of whipped foams. We have successfully applied the backlight-scattering technique to quantitatively measure the fat particle structure inside the food systems in a noninvasive way (7).

It has been generally accepted that interfacial properties such as surface and interfacial tension, diffusion, and adsorption–desorption properties of surfactants and proteins are of paramount importance to the stability of foam-based food products (4,8–13). Researchers have expended much effort in determining the static and dynamic interfacial properties, and a number of methods exist to study that. However, all of these methods are based on the concept that the foam or emulsion stability is controlled by the interfacial properties of a single interface in isolation. However, several of the interfaces are in close proximity to the surfaces in these aerated emulsion systems, with a film of only a few nanometers to almost a few micrometers in thickness. Under these conditions, there are interactions occurring across the film that can be significant. Toward this end, we have recently developed a new noninvasive method to measure the static and dynamic properties of the foam and emulsion films (14–18).

Dispersed air may degrade in many ways; for example, it may degrade through aggregation, creaming, coalescence, or Ostwald ripening and gas diffusion (19). Ostwald ripening is the process by which larger bubbles grow at the expense of the smaller ones because of differences in their chemical potential. The growth occurs by the diffusion of the dispersed phase through the continuous phase. Lifshitz and Slezov (20) and, independently, Wagner (21) developed an analytical solution for the Ostwald ripening process for a dilute dispersed phase. Gas diffuses out of the system in an open system where the dispersed phase is gas, and it results in a decrease in the bubble

size and overrun. De Vries (22,23) and Princen et al. (24,25) have provided the basic framework for studying gas diffusion to the atmosphere. Prins (26) showed the effect of the viscoelasticity of the bubble surface on the rate of gas diffusion. Recent studies (27–29) have been done to understand the effect of bulk rheology on bubble dissolution. However, very little work has been done to understand the effects of gas diffusion and Ostwald ripening on the stability of aerated food emulsions.

The purpose of this chapter is to provide quantitative descriptions of the fat particle structure variation during the whipping process using the backlight-scattering technique and to relate this structure to the stability of the whipped products. This research also attempts to interpret the dynamic film tension, film elasticity, and film thickness stability of foam-based products and to understand the effects of Ostwald ripening and gas-diffusion mechanisms on the long-term stability of aerated food products.

II. MATERIALS AND METHODS

A. Emulsion Preparation and Whipping

The emulsion preparation is as follows: Sodium caseinate, emulsifiers (poly-sorbate 60 and sorbitan monostearate), and gums (xanthan and guar) were dispersed in water. Partially hydrogenated vegetable oil, syrups, and flavors were then added to make a preemulsion, which was then pasteurized and homogenized in a two-stage homogenizer. The resulting emulsion was cooled to 1–3°C and aged for 45 min in a tank at about 5°C to produce the final emulsion samples used in this study. Air was injected into the aged emulsion under pressure, and the mixture was whipped under high stress for 15 min. The final whipped foam was produced after equilibrium was reached inside contherm 1 and contherm 2 (Fig. 1). Two food emulsion samples were prepared by this method. The fat concentrations in these two samples are 12 wt% and 20 wt%, respectively.

The sizes of the fat particles inside the food emulsion samples were measured using a Horiba LA-900 particle size distribution analyzer (Horiba Instruments Incorporated, Irvine, CA). The fat particle sizes in these two food emulsion samples were nearly the same (mean particle size around 0.4 μm).

B. Mesophase Preparation

The aerated mesophase was chosen as a model system to study the role of gas diffusion and Ostwald ripening on the stability of an aerated food system. The mesophase consisted of 2 wt% surfactant,

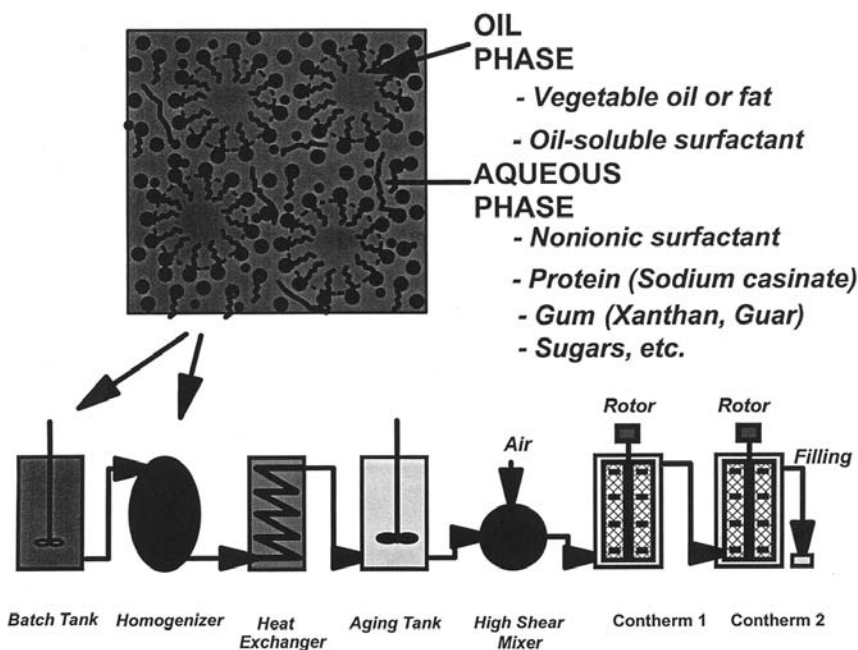


Figure 1 Sketch of typical food emulsion and foam process.

33 wt% sugar, and 65 wt% water. We chose propylene glycol stearate [hydrophile-lipophile balance (HLB): 1.8; molecular weight (MW): 387] and triglycerol stearate (HLB: 7.2; MW: 568) as low-HLB surfactants and sucrose stearate (HLB: 15; MW: 652) as a high-HLB surfactant. A low-HLB surfactant is dry mixed with sucrose stearate in the desired proportions (i.e., a high-HLB to low-HLB surfactant molar ratio was kept as 0.56) and added, under vigorous stirring, to water maintained at a temperature of 80°C. The total surfactant concentration was kept at 6 wt%. The surfactants were mixed for about 15 min in order to ensure the complete dissolution of the surfactants in the solution. The mesophase was refrigerated overnight prior to use. At the time of the experiment, the mesophase was mixed with equal weights of sugar and water. The mesophase was whipped using a Hobart (N-50) whipping machine. Whipping was done for 1 min at low speed followed by a high speed of aeration for 2 min at room temperature (22–25°C). The aerated mesophase was stored at room temperature and in refrigerated conditions. We measured the bubble size distribution and overrun as a function of time in order to describe the destabilization process quantitatively.

C. Backlight-Scattering Experiment

The nondestructive backlight-scattering technique has been successfully applied to obtain the information of the particle structure and interparticle interactions inside colloidal dispersions in our previous research (7,30). In this research, the backlight-scattering technique was used to obtain the information about the particle structure variation under and after the shear stress. Figure 2 illustrates the experimental setup: a collimated green light beam (50 μm in diameter, wavelength 543 nm) produced by a 0.5-mW He-Ne laser (Model 155A, Spectra-Physics Laser Products, Mountain View, CA) was scattered by colloidal particles inside the sample under a controlled temperature and produced a scattering image on the surface of a glass vial. The image intensity was then recorded by a vertically polarized coupled-charge device (CCD) digital camera (Lynxx 2000 Frame 336*244FT, Spectra Source Instruments, Westlake Village, CA) and downloaded to a

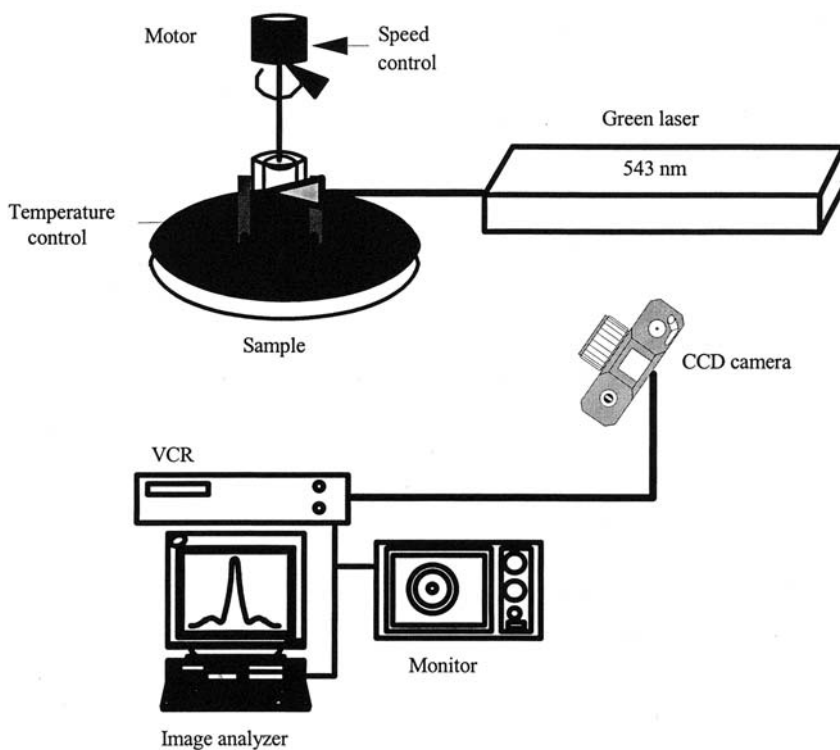


Figure 2 Backlight-scattering experimental setup.

computer (IBM-compatible PC Pentium/120 MHz). The recorded image was transformed into an intensity profile by image-analyzing software (Lynxx 2000, Version 3.04b, Spectra Source Instrument, Westlake, CA). According to our previous research (7), the value of the normalized structure factor $S(Q)$ [which is defined as the structure factor $S(Q)_{\max}$ at the first maximum point divided by the structure factor $S(Q)_{\min}$ at the first minimum point] can be used to quantify the fat particle structure inside food emulsions due to the decreased oscillatory behavior of the structure factor against the scattering vector. Larger values of $S(Q)$ yield more ordered structures inside colloidal dispersions.

D. Film Rheology and Film Thickness Stability

When the bubbles or droplets interact in a foam or emulsion system, a film is formed from the continuous phase between the bubbles or drops. The stability of any foam or emulsion depends on the response of the thin liquid film and the Plateau borders during shear and dilatation. In real polydispersed foam and emulsion systems, thin liquid films formed between bubbles or drops are not flat, but have a spherical curved shape. We developed a dynamic film tensiometer (Fig. 3) to study the film's rheological properties and thickness stability (14–18, 30,31). A small drop of emulsion (15–20 μm in size) is placed at the tip of a glass capillary (0.6 mm of inner diameter and 0.05 mm of wall thickness) and a drop with a double meniscus is formed. The capillary is connected to a feed syringe with a piston having a fine screw. A curved, spherical, cap-shaped film is formed with its meniscus adhering to the capillary drop by expelling the emulsion using air (Fig. 3). The diameter of the film for the foam lamella is slightly larger than the capillary diameter. Because the inner and the outer parts of the foam are air, the surface of the foam lamella is a part of a sphere. A sensitive pressure transducer (with sensitivity of $\pm 0.25 \text{ dyn/cm}^2$) was used to measure the capillary pressure versus time. The output of the pressure transducer is fed into a computer using a data acquisition card. The size of the film is controlled (i.e., expanded or contracted) by the feed syringe.

The interfacial film tension (f) is related by the Young–Laplace equation to the film radius (R_f) and capillary pressure (P_c) as

$$P_c = \frac{2f}{R_f} \quad (1)$$

The film tension is equal to the two times the single interfacial tension because the film consists of two single interfaces.

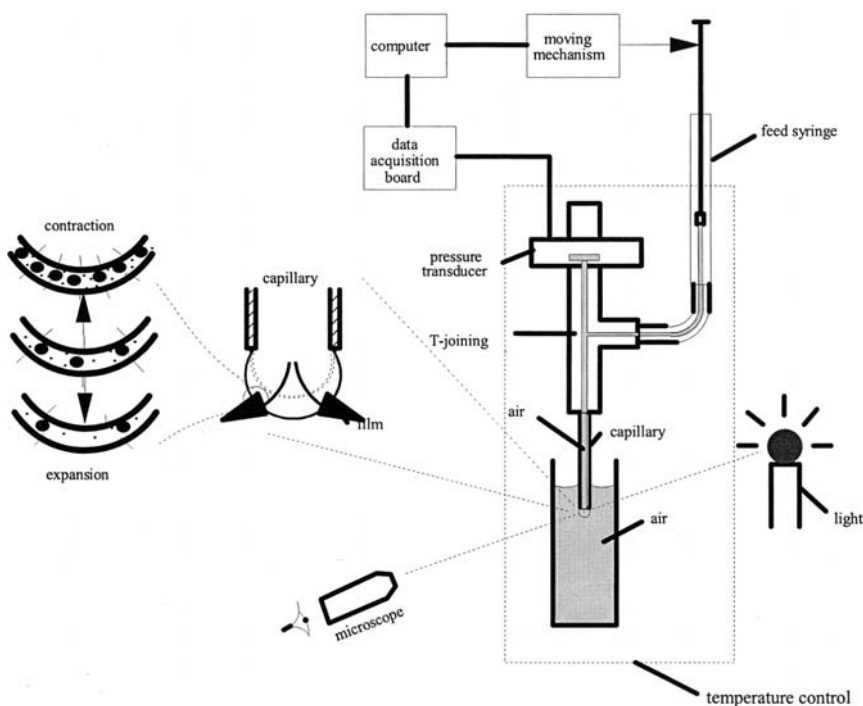


Figure 3 Diagram of the film rheometer.

Dynamic experiments are usually conducted by either expanding or contracting the film area. In the film stress–relaxation experiments, the film is quickly expanded or contracted, and then the relaxation of the film tension (capillary pressure) is measured. During this process, the film area is kept constant. When the film area expands, the surfactant concentration on the film surfaces drops. The film tension and the capillary pressure jump from the equilibrium value of the surface tension to the value corresponding to the new area per surfactant molecule on the film surfaces. The surfactants in the meniscus and in the film start to adsorb to restore equilibrium and, thus, the capillary pressure and film tension decreases as time progresses and finally approach an equilibrium value. The initial film tension (f_i) versus the logarithm of the relative film expansion area provides information about Gibbs film elasticity as follows:

$$E_f = \frac{df_i}{d \ln(A/A_0)} \quad (2)$$

where A_0 is the initial film area.

Our film rheometric technique also allows for the study of the dynamic film thickness stability of curved films. Due to the decreased surfactant concentration on the film expansion surface, critical film expansion ratio exists, and after that, the films will rupture.

E. Foam Film Air Permeability

The stability of foam-based food products depends on the air permeability throughout the foam lamella (32). In order to measure the foam film air permeability, a curved, spherical, cap-shaped foam film was formed at the tip of a glass capillary (0.6 mm inner diameter and 0.05 mm wall thickness), and the foam bubble diameter and capillary pressure were monitored versus time. The temperature was kept constant at 5°C during the measurement. Foam film permeability can be calculated by using the air flow rate, capillary pressure, foam lamella area, viscosity, and foam lamella thickness. The foam film tension measurement by the film rheometer provides simultaneous information about the capillary pressure, gas flow rate, and foam lamella area as a function of time. The gas flow rate (q) throughout the foam lamella is related by the Darcy equation to the film area (A), the capillary pressure (P_c), viscosity μ , foam lamella thickness (h), and permeability (k) (33):

$$q = k \left(\frac{AP_c}{\mu h} \right) \quad (3)$$

When the foam lamella is formed on the tip of capillary, the lamella thins. During that time, the air diffuses throughout the foam lamella and the foam cell shrinks. The foam lamella increases its thickness due to the viscosity effect during the shrinking. The rate of the foam cell shrinking process is modeled assuming that the film thinning rate (V_f) follows Reynolds law:

$$V_f = \frac{2h^3 F}{3\pi\mu r_1^4} \quad (4)$$

where r_1 is the film radius of the curved film, h is the film thickness, and F is the capillary force. As the film drains, the thickness decreases from the initial thickness h_1 to thickness h_2 . The time that the film thickness decreases from h_1 to h_2 is given by the Reynolds equation:

$$t_{12} = \frac{3\pi\mu r_1^4}{4F} \left(\frac{1}{h_2^2} - \frac{1}{h_1^2} \right) \quad (5)$$

Assuming that the total film volume is constant during foam cell shrinking (i.e., high film viscosity as in food emulsions samples), then

$$h_2 = \frac{R_1 L_1 h_1}{R_2 L_2} \quad (6)$$

where R_1 is the foam cell radius before shrinking, R_2 is the foam film radius after shrinking, L_1 is the foam cell height before shrinking, and L_2 is the foam cell height after shrinking.

Combining Eqs. (5) and (6), the film thickness of the shrinking foam film as a function of time can be derived as

$$h_2 = h_{2,\text{drainage}} + h_{2,\text{shrinkage}} - h_1 \quad (7)$$

where

$$h_{2,\text{shrinkage}} = \frac{R_1 L_1 h_1}{R_2 L_2} \quad (8)$$

and

$$h_{2,\text{drainage}} = \left(\frac{1}{h_1^2} + \frac{4\Delta t_{12} P_c A_f}{3\pi\mu r_1^4} \right)^{-1/2} \quad (9)$$

F. Measurement of Overrun and Bubble Size

Overrun of the mesophase is defined by the percentage of incorporated air with respect to the initial mesophase volume. Incorporated air reduces the density of the mesophase. The amount of incorporated air can be estimated by measuring the change in the density of the mesophase. Measurement error was estimated to be about 5–10% in this method. However, this is an absolute error (i.e., if the overrun is 1000%, then the confidence interval is 990–1010%). Bubble size distributions were measured from the video frames using a transmitted light microscope and VCR, and diameter measurements were taken using ImagePro Software (images from the videotape can be captured by this software). These captured images can be analyzed automatically or manually. Bubbles are clearly seen in this image. We used the manual mode to measure the diameter of the bubbles; one can accurately measure bubbles having a diameter of 1 μm or more. (The presence of smaller bubbles can be observed visually.) Aerated samples were sandwiched between a glass slide and a thin glass plate. The thin glass plate was very light and probably did not affect the bubble shape as only a very small number of distorted bubbles were observed. This is probably the result of

the high elasticity of the mesophase, which could sustain the weight of the thin glass. As an additional measure, we measured the diameters of bubbles that appear distorted and took the average. We then focused on a single plane of the mesophase. The bubbles from the other planes are out of focus and cannot be seen very clearly. We did not measure the bubbles that were out of focus. A substantial number of bubbles (100–150) were counted in each frame. In order to obtain statistical estimates of bubble size distribution, 6–10 frames (containing a total of about 800–900 bubbles) were used.

G. Measurement of Gas Diffusion

The rate of air loss from a single bubble is measured to quantify the gas loss (decrease in overrun) from the system. A bubble is formed inside the liquid (i.e., mesophase) and the diameter of the bubble is measured as a function of time. This would give an idea of the permeability of the surfactant film to air and permeability of air through the liquid medium. The pressure difference between the bubble and the atmosphere is the main cause for gas transfer from the bubble to the atmosphere. The rate of gas loss depends on the size of bubble, the surface tension of the liquid, the permeability of the liquid film, and the distance from the free gas–liquid surface. Air bubbles are either at the gas–liquid interface or in the bulk liquid. In order to simulate an aerated mesophase, we decided to study two cases: (I) gas diffusion from a bubble when the bubble is at the gas–liquid interface and (II) gas diffusion from a bubble when the bubble is inside the bulk liquid. The bubble shrinks over time when the bubble is formed at the gas–liquid interface. Let us imagine that a bubble of radius r is formed at the gas–liquid interface. The pressure difference between the bubble and the atmosphere will be

$$\Delta P = \frac{2\sigma}{r} \quad (10)$$

where σ is the surface tension.

Now, the concentration difference can be expressed in terms of the pressure difference. If we combine the above equation with the ideal gas law and Fick's law of diffusion, the following equation (24) can be obtained:

$$r^2 = r_0^2 - 4\alpha \left(\frac{D\sigma}{hP_0} \right) t \quad (11)$$

where r is the radius at the instant time t , r_0 is the initial radius, P_0 is the atmospheric pressure, D is the diffusivity of the film, h is the thickness of the film, σ is the surface tension, and α is the dimensionless factor (24). α is a measure of the area of the bubble that is exposed to the air directly above

the plane of contact with the liquid. This equation relates the radius of a shrinking bubble with time. Almost all of the gas diffuses through the film area when the bubble is at the gas–liquid interface (directly exposed to the atmosphere). The rate of gas diffusion depends on the area of the film, the thickness of the film, and the film structure (molecular packing in the film).

The physics of the problem remains the same when the bubble is inside the bulk liquid. Let us imagine that a bubble of radius r is placed inside the liquid at a distance h from the gas–liquid interface. If we neglect the pressure exerted by the liquid height h , the pressure difference between the bubble and the atmosphere can be expressed by Eq. (10). The concentration difference can be expressed in terms of the pressure difference using Henry's law. By combining Eqs. (10) and (11) with the ideal gas law and Henry's law, we obtain

$$r^2 = r_0^2 - 4 \left(\frac{RT}{P_0} \right) \left(\frac{DS\sigma}{h} \right) t \quad (12)$$

Equation (12) relates the radius of a shrinking bubble with time when the bubble is inside the liquid; S is the solubility of the dispersed phase (air) at the interface.

A bubble is formed inside the mesophase using the setup described in Fig. 4 in order to measure the gas diffusion from a bubble inside the mesophase. The bubble is kept at a fixed distance from the air–mesophase interface using a thin glass plate. The distance of the bubble from the air–mesophase interface was approximately 250 μm . The diameter of the bubble is measured as a function of time to determine the rate of air loss from a single bubble.

III. RESULTS AND DISCUSSION

A. Fat Particle Structure Variation During Homogenization

Homogenization is responsible for the formation of food emulsions. The structure factor was measured immediately after homogenization for three emulsions containing 5 wt%, 12 wt%, and 20 wt% fat. Figure 5 shows that the structure factor for all the samples was approximately 1, indicating that a very poor fat-particle-packing structure was produced after homogenization; therefore, all of the food emulsions were unstable.

The temperature is very high after homogenization (around 72.5°C). Xu et al. (7) observed that a food emulsion become less stable with an increase in temperature. Figure 5 also reveals that the fat-particle-ordering structure was better (more than 1) for an emulsion containing 20 wt% fat.

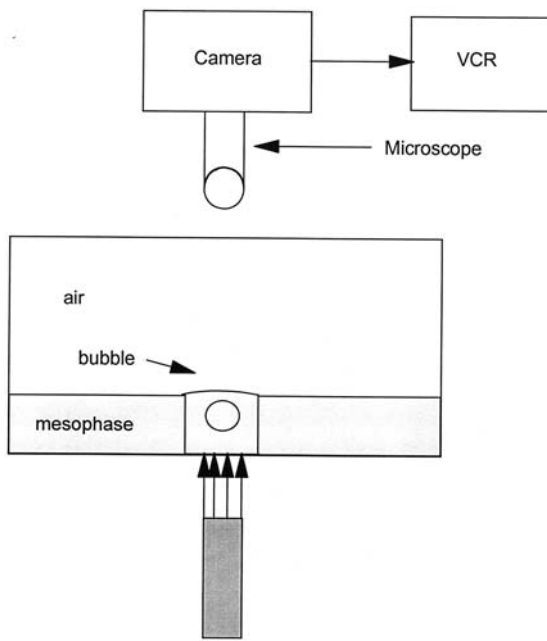


Figure 4 Experimental setup for the single-bubble experiment.

The fat particle concentration inside a 20-wt% fat emulsion was much higher than that of other two samples and the increased fat particle concentration probably resulted in improved fat particle structure.

B. Fat Particle Structure During Cooling

The emulsions were cooled to nearly 5°C to prevent fat particle aggregation or coalescence after homogenization. The fat particle structuring factor greatly improved after cooling the three samples when compared with the particle size distribution after homogenization. It was found that the particle size distribution remained unchanged in all three samples. The normalized structure factor for an emulsion containing 20 wt% fat is shown in Fig. 6. Increased fat particle structuring suggests that the food emulsions should be cooled down immediately after homogenization to avoid fat particle aggregation or coalescence. The particle size distribution for all three samples remained unchanged. Starch particles were added after cooling and before aging. The fat particle structure becomes less ordered due to the addition of large starch particles for the 5-wt% fat whipped foam. The effect of starch particles and fat destabilization has been systematically

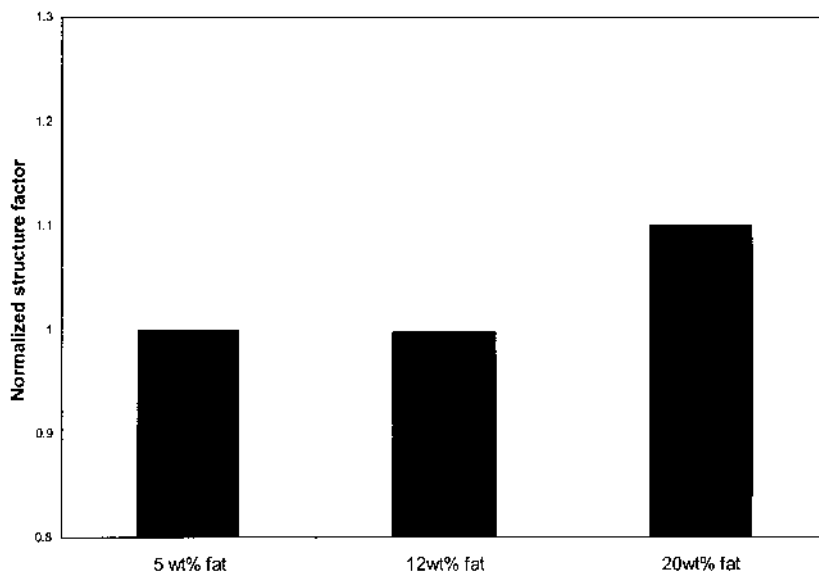


Figure 5 Normalized structure factor after homogenization.

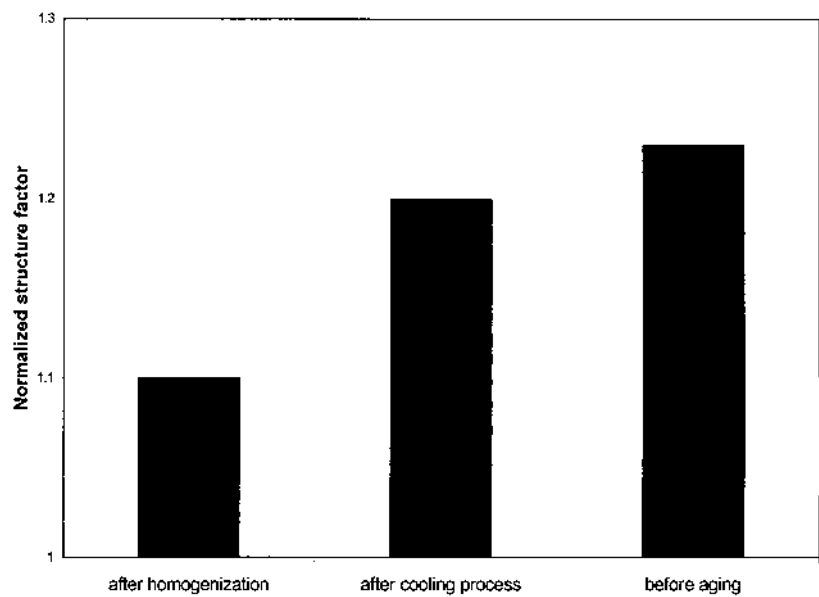


Figure 6 Normalized structure factor after cooling for an emulsion containing 20 wt% fat.

studied by Xu et al. (7). It was found that the effect of starch on the fat particles was similar to that of particle polydispersity. Increased particle polydispersity decreased the particle ordering (7), and the stability of the food emulsion decreases.

The fat particle structure for the 12-wt% fat and 20-wt% fat whipped foams are slightly greater than the other sample and benefited from the adsorption of surfactants and proteins on the fat particle structure. However, the increase in the fat particle structuring was small, implying that most of the adsorption of surfactants and protein on the fat particle surface was completed before aging.

C. Fat Particle Structure During Aging

It was observed that the fat particle structure for emulsions containing 5-wt% and 12-wt% fat did not change with aging time. For an emulsion containing 20 wt% fat, a small and gradual increase was observed (Fig. 7). No significant change was observed in the fat particle size distribution during the aging process. Some studies (4,34) have concluded that one

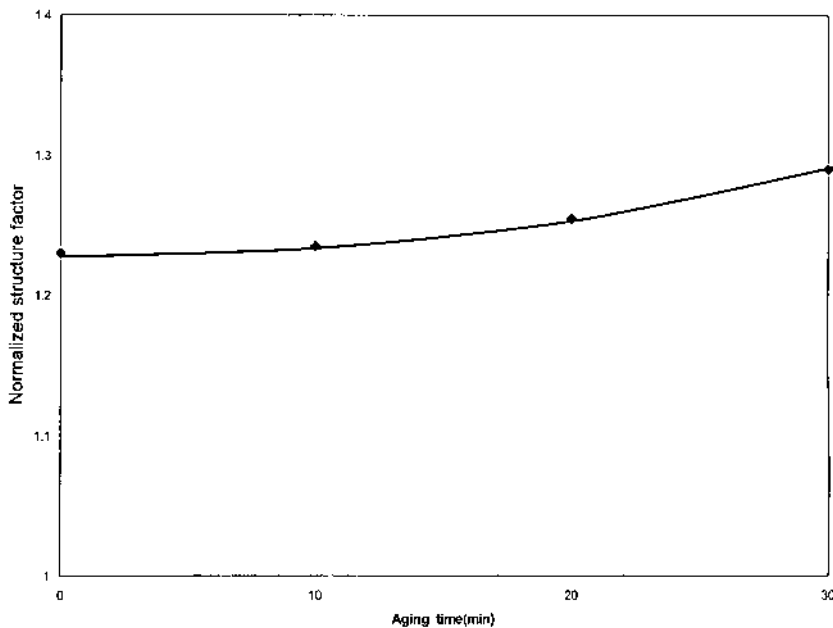


Figure 7 Fat particle structure variation during aging for an emulsion containing 20 wt% fat.

important role of aging was to provide the necessary time to achieve the complete coverage of fat globules with adsorbed molecules and competitive adsorption between surfactant and proteins. However, our results suggest that most of the adsorption of surfactant and proteins was completed before the aging process. Based on our observations and the results of the other studies (4,34), the role of aging can be summarized as follows:

1. The polysaccharide stabilizers, such as gums, require time for full hydration; therefore, the bulk viscosity increases with the aging time.
2. The crystallization of fat particles occurs during the aging process. According to Darling and Goff (34), the existence of crystalline fat inside fat particles was important to the whippability of food emulsions. They found that without the crystalline phase, the undesired coalescence of fat droplets occurs during the whipping process, and the resulting whipped foams are unstable.

D. Fat Particle Structure During Aeration

It was observed that the fat particle structure inside the low-fat emulsions (5 wt% and 12 wt%) did not change during the aeration process. However, the fat particle structure inside the high-fat product (20% fat) decreased. This is probably the result of the increased collision between the fat particles at high fat concentrations due to high mechanical agitation. Increased fat particle collisions resulted in flocculation and clustering, which, in turn, reduced the fat-particle-ordering structure.

E. Fat Particle Structure During the Whipping Process

It was observed that the fat particle structuring was greatly improved (Figs. 8–10) during the whipping process, indicating a well-developed fat particle structuring in the bulk phases. It is worth noting that the normalized structure factor after whipping in our samples is found to be the same as the sequence of stability of whipped foam products (i.e., 20 wt% fat whipped foam > 5 wt% fat whipped foam > 12 wt% fat whipped foam), indicating that many factors, such as fat particle attachment at the air–water interface and the formation of a three-dimensional fat particle network structure between neighboring air bubbles, can influence the stability of whipped foams. The developed fat particle structure in the bulk phase after whipping is one of the most important factors in determining the stability of whipped foams.

The data shown in Figs. 8–10 also indicate that in a stable whipped foam, most of the fat particles in the bulk phase remain in a single particle

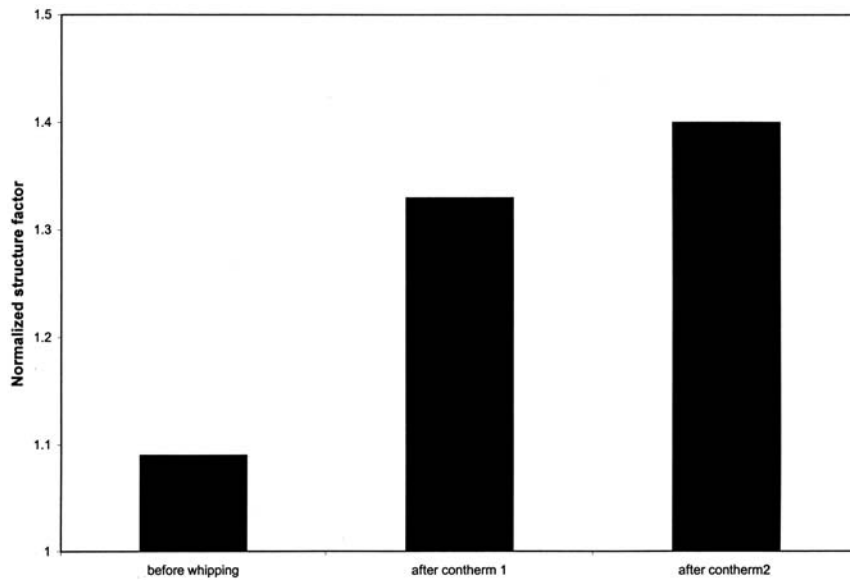


Figure 8 Fat particle structure variation during whipping process (for an emulsion containing 5 wt% fat).

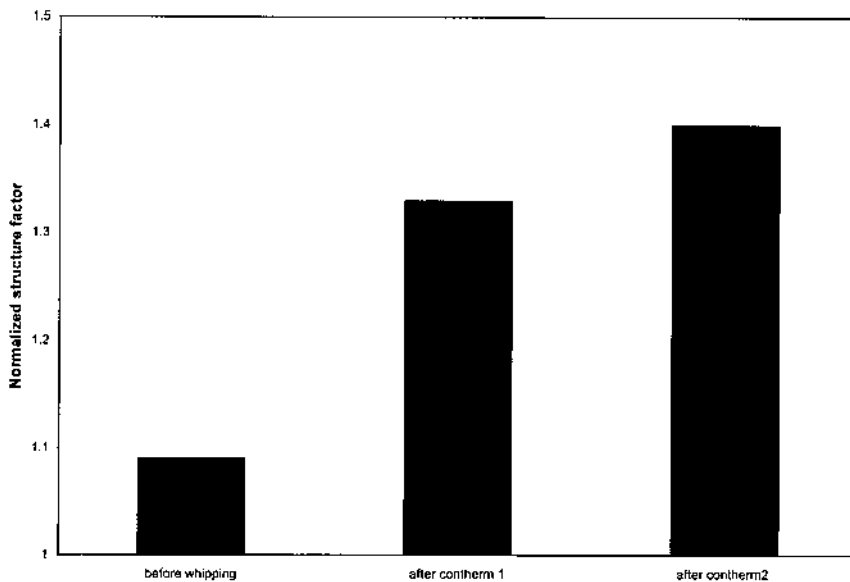


Figure 9 Fat particle structure variation during whipping process (for an emulsion containing 12 wt% fat).

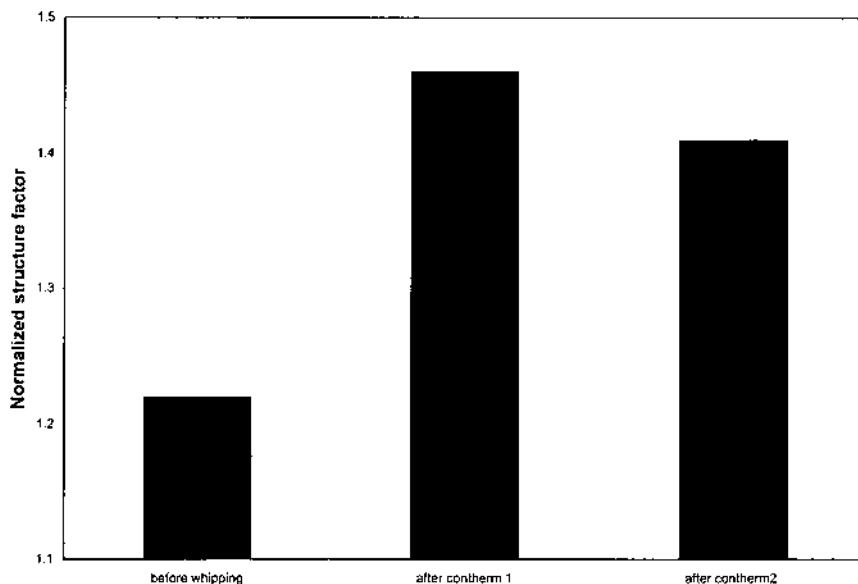


Figure 10 Fat particle structure variation during whipping process (for an emulsion containing 20 wt% fat).

state and are well distributed in space, rather than being flocculated, clustered, clumped, or even coalesced to form large particles. The effect of fat particle floccules, clusters, clumps, or coalesced fat particles on the fat particle structure is similar to the addition of particle polydispersity. When fat particle aggregation occurs, the fat particle structure should become less ordered (7). Other researchers reached a similar conclusion using various techniques (2,3,5,6,11). They found that the outline of the individual fat globules and clusters in a stable whipped foam were clearly observable; in the unstable dairy foam, the fusion/coalescence of fat particles was observed.

Controlled fat particle destabilization is necessary in order to produce stable whipped foams. For example, before fat particles can attach to the air-water interface or the three-dimensional fat particle network structure can form between neighboring air bubbles, the fat particles have to be ruptured or destabilized (clustered or clumps). The fat particle destabilization during the whipping process should be optimally controlled to produce a stable whipped foam. The fat particle structure decreased with the increasing fat particle concentration in the second whipping stage (contherm 2). In fact, the fat particle structure decreased for the 20-wt% fat whipped foam, indicating that too many fat particles were destabilized and overwhipping

occurred. In this case, only one whipping stage is necessary for high-fat products.

The stability of the whipped foams depends on the interactions between the fat globules and air bubbles. This leads to the buildup of a matrix in which air bubbles are stabilized. The initial stage of the whipping process involves the adsorption of protein and surfactants onto the air–water interface. This gives an initial stabilizing effect on the foams. Subsequent phases of the whipping process involve a progressive increase in the extent to which the fat particles are whipped to attach at the air–water interface, the formation of a fat particle structure in the bulk phase, the buildup of a three-dimensional network structure between neighboring air bubbles, and changes in the number and the size of the air bubbles. The periphery of each air cell in fully whipped foams is composed primarily of fat globules (5), but there is also a variable amount of original protein adsorbed at the air–water interface. The rigidity of the foam structure is provided by bridges of clustered fat particles connected to adjoining air cells and by the formation of a well-developed fat particle structure in the bulk phase.

F. Film Tension, Elasticity, and Thickness Stability

The film elasticity and dynamic film stability of two types of fat-in-water emulsions were investigated: a 12-wt% fat-in-water emulsion and a 20-wt% fat-in-water emulsion. Figures 11 and 12 show the data of foam film stress relaxation with a relative film area expansion of 26%, 46%, and 66% for the 20-wt% fat-in-water emulsion and the 12-wt% fat-in-water emulsion, respectively. Initially, the film was expanded very quickly; the surfactant concentration on the film surface suddenly decreased due to the increased film area. As a consequence, the film tension jumped from its equilibrium value to the maximum value. After that, because the concentration of surfactants in the meniscus was higher than that of in the film, the surfactants diffused from the meniscus to the inside of the film, and from the inside of the film to the film surface; as a consequence, the film tension decreased and finally reached the equilibrium film tension (in approximately 15 min). Figures 11 and 12 show that the equilibrium values of the foam film tension of 20 wt% and 12 wt% fat-in-water emulsions are both approximately 91 dyn/cm. However, the initial value of the film tension right after the expansion and the value of the initial slope of the curved film tension versus time were different (Figs. 11 and 12). These data are presented in Table 1. Based on the data, the film elasticity was calculated for the 20-wt% fat and 12-wt% fat foam films formed from the corresponding emulsions (Fig. 13). The film elasticity data show that the 20-wt% fat foam film had a

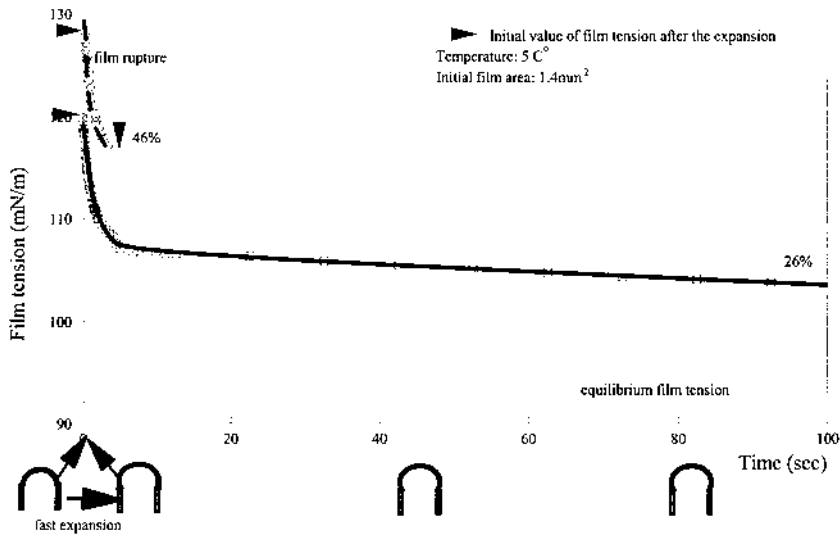


Figure 11 Foam film stress relaxation with relative film expansion area: 26% and 46% for fat-in-water emulsion (fat concentration: 12 wt%).

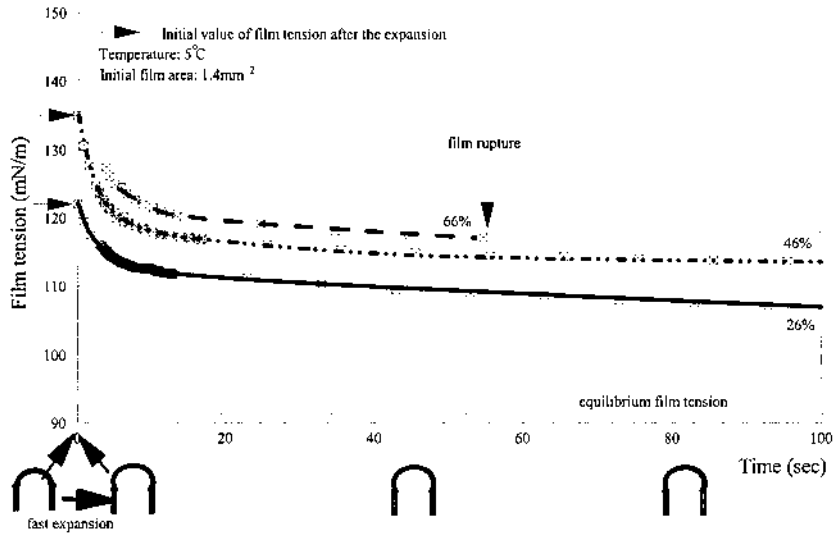
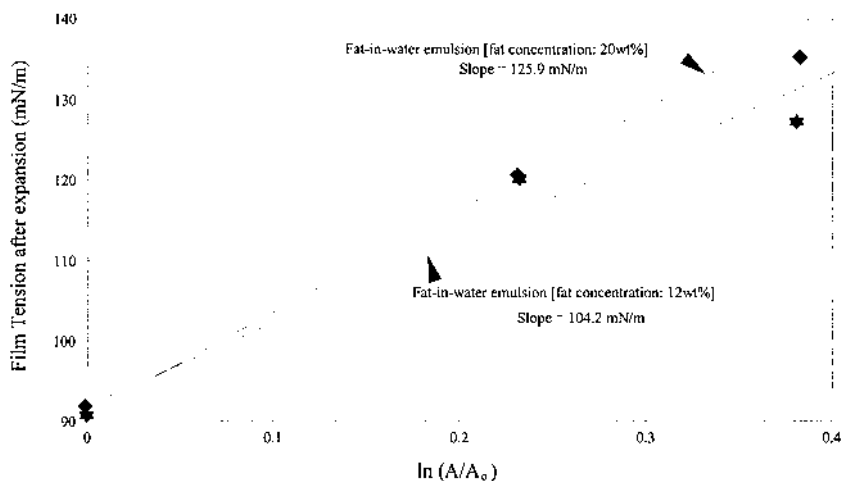


Figure 12 Foam film stress relaxation with relative film expansion area: 26%, 46%, and 66% for fat-in-water emulsion (fat concentration: 20%).

Table 1 Foam Film Rheological Properties

Sample	Equilibrium film tension (mN/m)	Initial slope of the curved film tension versus time (26% expansion) (mN/m s)	Gibbs film elasticity (mN/m)
20 wt% Fat-in-water emulsion	91	-12.7	125.9
12 wt% Fat-in-water emulsion	92	-25.0	104.2

**Figure 13** Foam film elasticity for fat-in-water emulsions.

higher film elasticity, indicating that the 20-wt% fat foam film should have a higher dynamic film stability. This showed a good correlation with the stability sequence of whipped foams produced from the corresponding food emulsions (i.e., 20 wt% fat whipped foam > 12 wt% whipped foam).

It is also found that the initial slope of the curves shown in Figs. 11 and 12 for the 12-wt% fat-in-water emulsion was higher than the slope for the 20-wt% fat-in-water emulsion, indicating that the diffusion rate of surfactants (polysorbate 60) in a 20-wt% fat-in-water emulsion was slower than that of the 12-wt% fat-in-water emulsion. The Marangoni–Gibbs effect on the stability of foam films was more pronounced for the 20-wt%

fat-in-water emulsion sample, and the foam film produced from 20-wt% fat-in-water emulsion should be more stable. This shows a good correlation with the stability sequence of whipped foams produced from the corresponding food emulsions.

Additionally, the film expansion ratios that the two systems could tolerate without rupturing were different. No rupture for the 20-wt% fat system was observed in the course of the experiments for the expansion ratios of 26% and 46%; the 12-wt% fat system was stable and ruptured only at 26% expansion. This film ruptured in about 3 s at a 46% expansion ratio. The 20-wt% fat system withstood a 66% expansion ratio for 57 s. In this experiment, the initial foam film area was 1.4 mm² for all samples. The data show the same conclusion as the elasticity measurement that the foam film produced from the 20-wt% fat-in-water emulsion—it had a higher dynamic stability than that produced from the 12-wt% fat-in-water emulsion.

We have observed a similar correlation between the foam film elasticity and the stability of the whipped dairy cream emulsion using polyglycerin fatty acid ester and sucrose ester as emulsifiers (35). It was found that at the same mole of emulsifiers (3.3×10^{-4} M) the emulsion containing 30 wt% fat and polyglycerin fatty acid ester had a film elasticity of 57.8 dyn/cm compared to 46.5 dyn/cm for the emulsion containing sucrose ester, thereby demonstrating that greater stability results from a higher film elasticity.

G. Foam Film Air Permeability

The stability of aerated emulsions also depends on the air permeability throughout the foam (32). Figure 14 presents the experimental foam bubble diameter as a function of time for the 20-wt% fat-in-water emulsion and the 12-wt% fat-in-water emulsion. The initial foam bubble diameter was 1 mm for both samples. The rate of bubble shrinkage for foam lamella formed from the 12-wt% fat-in-water emulsion was about 1.5 times faster than that of lamella formed from the 20-wt% fat-in-water emulsion. Similar observations were made when the experimental capillary pressure, foam film surface area, and foam volume were plotted as a function of time.

The calculated foam lamella permeability/film thickness for the fat-in-water emulsion systems is presented in Fig. 15. The value of the foam lamella permeability/film thickness for the 12-wt% fat-in-water emulsion has a maximum (15×10^6 darcy/cm) at 150 min. The data for the 20-wt% fat-in-water emulsion are almost in a straight line. At a film thickness of 200 nm, the foam lamella formed from the 12-wt% fat-in-water emulsion at 150 min has an air permeability of about 50 darcy; under the same conditions, the foam lamella formed from the 20-wt% fat-in-water emulsion has a permeability of about 5 darcy (10 times lower). One can conclude that

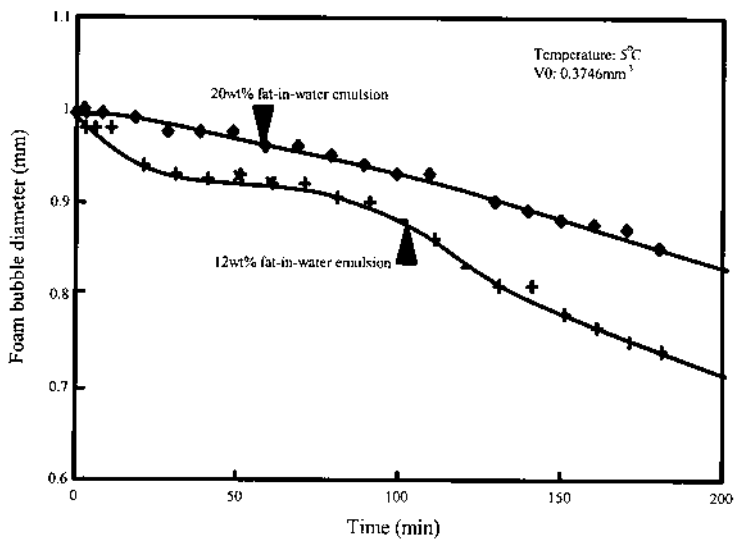


Figure 14 Experimental foam bubble diameter versus time for fat-in-water emulsions.

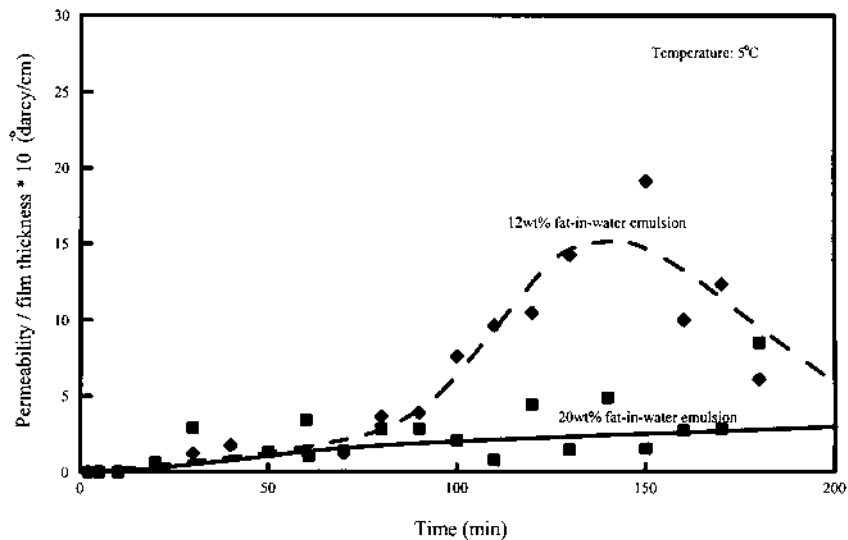


Figure 15 Foam lamella air permeability of fat-in-water emulsions.

smaller foam film permeability values result in greater stability in foam-based products.

H. Long-Term Stability of Model Aerated Food Emulsions

As discussed earlier, the dispersed air within the aerated food emulsions may degrade because of Ostwald ripening and the gas-diffusion process. The roles of these processes were studied using a model system (mesophase) before studying the effect of these processes on actual aerated food emulsion systems. In analyzing the long-term stability of the aerated mesophase, it is important to measure the change in the overrun and the change in the bubble size distribution over time. It must also be noted that the contribution of the large bubbles to the overrun is much more significant than the contribution from the small bubbles because the volume of air in a bubble of diameter d varies as d^3 . Therefore, it is more instructive to interpret the stability of the aerated mesophase using a plot of the volume distribution of bubbles rather than the number distribution. The bubble volume at each size for the samples after a period of 1 week was multiplied by the ratio of the final to initial overrun and is plotted for the propylene glycol stearate–sucrose stearate system and triglycerol stearate–sucrose stearate system (Figs. 16 and 17, respectively). In order to present the loss of air as a function of the bubble size distribution, the initial overrun was chosen as a benchmark. This kind of normalization accounts for the change in the overrun and brings all curves to the same basis (viz. the volume of the total system occupied by bubbles of different sizes). The volume distribution shifts to the large-size range and a significant fraction of the air is retained in bubbles in the size range of 70 μm or more for the propylene glycol stearate system (Figs. 16 and 17). Note that bubbles in this size range were absent to begin with; even after a period of 1 week, the bubbles of this size are small in number, but significant in their contribution to the gas volume. The practical implication of this effect is that this aerated mesophase will be less suitable for use in the food emulsion because the large bubble size will tend to phase separate under the effect of buoyancy. In comparison, the volume distribution of the triglycerol stearate system does not change as much with time (i.e., after 1 week) and the bulk of the air volume is retained in bubbles of nearly the same size range—as was the case initially. Second, it is to be noted that the change in the overrun over a period of 1 week is significantly more for the propylene glycol stearate system than it is for the triglycerol stearate system, implying that the former is less stable than the latter. Finally, it is of significance that the storage temperature does not affect the size distribution to a great extent, but affects the overrun. The change in the overrun is due to the diffusion of

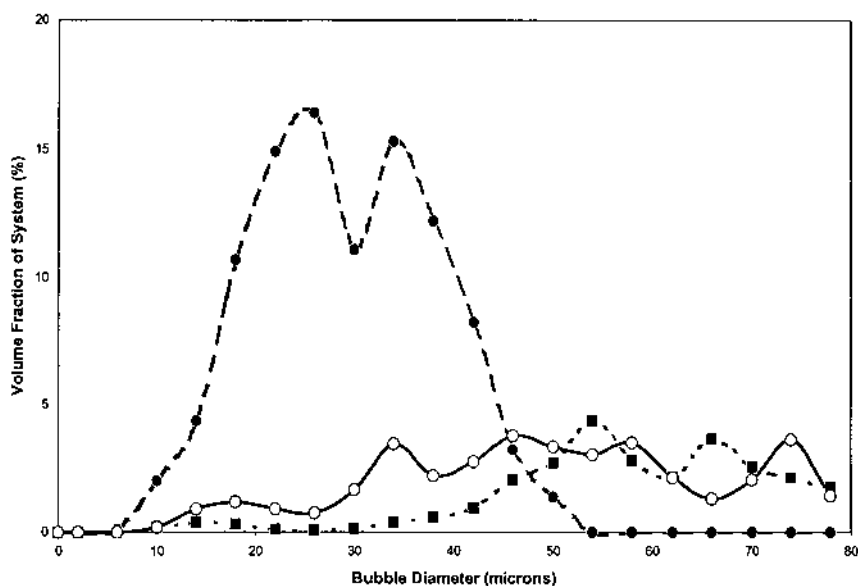


Figure 16 Long-term stability results for the propylene glycol surfactant system. The effect of temperature on volume distribution (corrected for overrun) of bubbles is shown. The solid circle (●) represents results just after whipping (overrun 1000%); the open circle (○) represents the results for the samples stored at 10°C for 1 week (overrun 320%) and the solid square (■) represents the results for samples stored at 25°C for 1 week (overrun 220%).

gas from the bubbles to the atmosphere. The rate of diffusion is greater at higher temperatures, resulting in the loss of more air from the aerated product and a lower overrun over a fixed period of time. The reason for the difference in the degree of air loss to the atmosphere between the two systems is due to the difference in the diffusivity of air in the two liquids.

1. Measurement of the Gas-Diffusion Rate

A bubble is formed inside the mesophase and the diameter of the bubble is measured as a function of time to determine the rate of air loss from a single bubble; this would give an idea about the rate of gas loss through the bulk liquid medium. The pressure difference between the bubble and the atmosphere is the main cause for gas transfer from the bubble to the atmosphere. The rate of gas loss depends on the size of the bubble, the surface tension of the liquid, the permeability of the liquid film, the distance

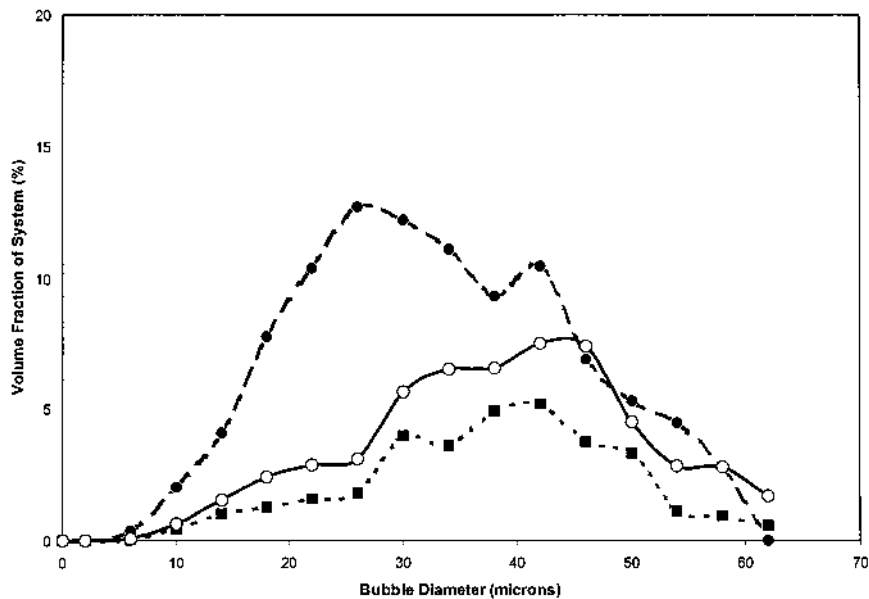


Figure 17 Long-term stability results for the triglycerol stearate surfactant system. The effect of temperature on volume distribution (corrected for overrun) of bubbles is shown. The solid circle (●) represents results just after whipping (overrun 820%). The open circle (○) represents the results for the samples stored at 10°C for 1 week (overrun 450%) and the solid square (■) represents the results for samples stored at 25°C for 1 week (overrun 270%).

from the free gas–liquid surface. Consider that a bubble of radius r_0 is placed inside the liquid at distance h from the gas–liquid interface. Pressure inside the bubble would be higher than the atmospheric pressure due to the capillary effect. This pressure difference would cause the gas to diffuse from the bubble to the atmosphere. De Vries (22,23) has modeled this phenomenon and related the radius of a shrinking bubble with time when the bubble is inside the liquid using the ideal gas law and Fick’s first law [Eq. (12)].

The slopes were 4.4 and $6.7 \mu\text{m}^2/\text{min}$ for the triglycerol stearate–sucrose stearate system and the propylene glycol stearate–sucrose stearate system, respectively, when the square of the radius was plotted as a function of time and the bubble was formed at a distance $250 \mu\text{m}$ from the free surface. Results suggest that the diffusivity of the gas from the propylene glycol stearate–sucrose stearate system is one and half times greater than that of the triglycerol stearate–sucrose stearate system. This explains the higher overrun loss for the propylene glycol system.

2. Ostwald Ripening Model and the Gas-Diffusion Model

A schematic of a section of aerated mesophase is shown in Fig. 18. Air bubbles are assumed to be surrounded by a layer of continuous medium of thickness δ and at a distance h_i from the free surface (i.e., the aerated system is in contact with the atmosphere, which we can imagine as a bubble of infinite radius). ϕ_{mi} , ϕ_{si} , and ϕ_∞ are the volume fraction of the gas phase in a continuous medium, at the bubble surface, and at the free surface, respectively. The difference in the concentration of the gas phase is due to the capillary pressure and the effect of the surrounding bubbles. The gas phase concentration in the continuous medium (ϕ_{mi}) can be assumed to be always greater than that at the free surface (ϕ_∞). This difference would lead to the transfer of gas from the continuous medium to the free surface. De Vries (22,23) has modeled gas transfer from a single bubble through a continuous medium to a free surface. ϕ_{mi} would be greater than the ϕ_{si} for bubbles larger than the critical radius and less than the ϕ_{si} for bubbles smaller than the critical radius. [Yarranton and Masliyah (36) have modeled the similar phenomena for the emulsion system]. Thus, air would be transferred from the continuous medium to bubbles larger than the critical radius and air would diffuse out of the bubbles smaller than the critical radius. The exchange of gas among the bubbles is called Ostwald ripening.

a. Ostwald Ripening. The change in radius of a bubble due to Ostwald ripening can be described by the following equations (36):

$$\frac{dr}{dt} = \frac{r(r + \delta)D}{r^2\delta} (\phi_{mi} - \phi_{si}) \quad (13)$$

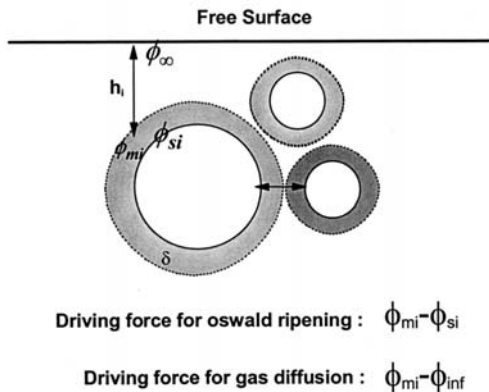


Figure 18 Schematic representation of the gas-diffusion and Ostwald ripening processes.

where D is the gas diffusion coefficient, r is the radius of the bubble, t is the time, and δ , ϕ_{mi} , ϕ_{si} are as defined earlier.

Yarranton and Masliyah (36) provided an expression for the dispersed-phase volume fraction in the continuous phase surrounding the droplet as a function of the droplet diameter and droplet size distribution:

$$\phi_{mi} = \phi_{si} + \frac{\alpha\phi_{\infty}\delta}{(r_i + \delta)} \left(\frac{1}{r_{10}} - \frac{1}{r_i} \right) \quad (14)$$

where r_{10} is the average bubble size (i.e., average radius of the bubbles) and α is defined as $\alpha = 2\sigma v_d / RT$, where σ is the interfacial tension between the two phases, v_d is the molar volume of the dispersed phase, R is a universal gas constant, and T is the temperature.

b. Gas Diffusion. Ostwald ripening does not predict any gas loss from the system. However, the overrun (i.e., amount of incorporated air) of the system decreases with time because of gas diffusion to the atmosphere. If Fick's first law is used to describe gas diffusion to the atmosphere from a bubble having radius r_i and at a distance h_i from the free surface, the following equation is obtained:

$$\frac{dN_A}{dt} = \frac{4\pi D(\delta + r_i)^2(\phi_{mi} - \phi_{\infty})}{h_i} \quad (15)$$

Now, because gas diffuses from the continuous medium surrounding the bubble, the dispersed phase volume will change:

$$\Delta\phi_{mi} = \frac{\Delta N_{Ai}}{\Delta V_i} \quad (16)$$

So, we can obtain

$$\frac{d\phi_{mi}}{dt} = \frac{3D(r_i + \delta)^2(\phi_{mi} - \phi_{\infty})}{h_i[3r_i\delta(\delta + r_i) + \delta^3]} \quad (17)$$

Using Eq. (14), we obtain

$$\frac{d\phi_{mi}}{dt} = \frac{d\phi_{si}}{dt} + \frac{d}{dt} \left[\frac{\alpha\phi_{\infty}\delta}{(r_i + \delta)} \left(\frac{1}{r_{10}} - \frac{1}{r_i} \right) \right] \quad (18)$$

$$\frac{d\phi_{mi}}{dt} = \frac{dr_i}{dt} \left[\frac{\alpha\phi_{\infty}}{r_i^2} - \frac{\alpha\phi_{\infty}\delta}{(r_i + \delta)^2} \left(\frac{2}{r_i} + \frac{\delta}{r_i^2} - \frac{1}{r_{10}} \right) \right] \quad (19)$$

Rearranging Eq. (19) and using Eq. (17), we can write

$$\frac{dr_i}{dt} = -g(\delta, \phi_\infty, r_i, r_{10}) \frac{3D(r_i + \delta)^2(\phi_{mi} + \phi_\infty)}{h_i[3r_i\delta(\delta + r_i) + \delta^3]} \quad (20)$$

where the function $g(\delta, \phi_\infty, r_i, r_{10})$ is defined as

$$\frac{1}{g(\delta, \phi_\infty, r_i, r_{10})} = \left[\frac{\alpha\phi_\infty}{r_1^2} - \frac{\alpha\phi_\infty\delta}{(r_i + \delta)^2} \left(\frac{2}{r_i} + \frac{\delta}{r_1^2} - \frac{1}{r_{10}} \right) \right] \quad (21)$$

Combining Eqs. (13) and (21), one can obtain the composite effect of Ostwald ripening and gas diffusion:

$$\frac{dr_i}{dt} = \frac{r(r + \delta)D}{r^2\delta}(\phi_{mi} - \phi_{si}) - g(\delta, \phi_\infty, r_i, r_{10}) \frac{3D(r_i + \delta)^2(\phi_{mi} - \phi_\infty)}{h_i[3r_i\delta(\delta + r_i) + \delta^3]} \quad (22)$$

3. Model Prediction

We observed that overrun decreases substantially over 1 week for both experimental systems. The bubble size distribution also changes significantly over the same period. Loss of gas could be attributed to the gas diffusion to the atmosphere. In order to obtain quantitative agreement, we simulated models for gas diffusion and the effect of Ostwald ripening. The simulation was conducted on 120,000 bubbles (with an initial size distribution that matches the experimental one) in a cylindrical vessel 12 cm in height. With this number of bubbles, the system volume that corresponds to an air volume overrun of 1000 vol% for propylene glycol system and 820 vol% for the triglycerol stearate system is a small fraction of the experimental system volume, although the simulation cell has the same height as the experimental system. This reduction in scale (i.e., smaller area) is necessary in order to keep the number of bubbles in the simulation manageable and it was found that this reduction in scale does not affect the results. For computational purposes, the cylinder was divided into 1200 layers. The thickness of a layer (100 μm) was chosen to accommodate the largest air bubble observed in the experiment.

a. Effect of Gas Diffusion on Overrun. The effect of gas diffusion on overrun (i.e., the long-term stability) was studied in two cases. In the first case, the De Vries model [Eq. (12)] was simulated for the bulk system. It was assumed that the radius of each bubble decreases with time as predicted by Eq. (12). The distance of each bubble from the free surface was known

because we had fixed the position of the each bubble in the vertical direction. The rate [slope of Eq. (12)] was obtained from the shrinking bubble experiments. The results of our simulations for the system are presented in Fig. 19. The De Vries (22,23) model predicts that the overrun of the triglycerol stearate–sucrose stearate system would decrease from 820% to 176% and the overrun of propylene glycol–sucrose stearate system would decrease from 1000% to 78%. However, for a finite dispersed-phase volume concentration, the gas-diffusion rate would be affected by the gas volume fraction and the bubble size distribution as described by Eq. (17). The simulation results are shown in Fig. 19. We did not see significant improvement when compared to the prediction of the De Vries (22,23) model. The results are understandable because our average bubble size was large (20 μm). When the bubble size is large, the contribution of the second term of Eq. (13) becomes negligible. This would make Eq. (17) the same as Eq. (12); both models predict almost the same decrease in the overrun for the system. When the average bubble size is small (as much as 5 μm), we observed a significant difference (as much as 50%) between the predictions of the De Vries model and Eq. (20).

b. Effect of Ostwald Ripening on Overrun. We observed the theoretical predictions were lower than the experimental observations when only the effect of gas diffusion was taken into account (overrun decreases from

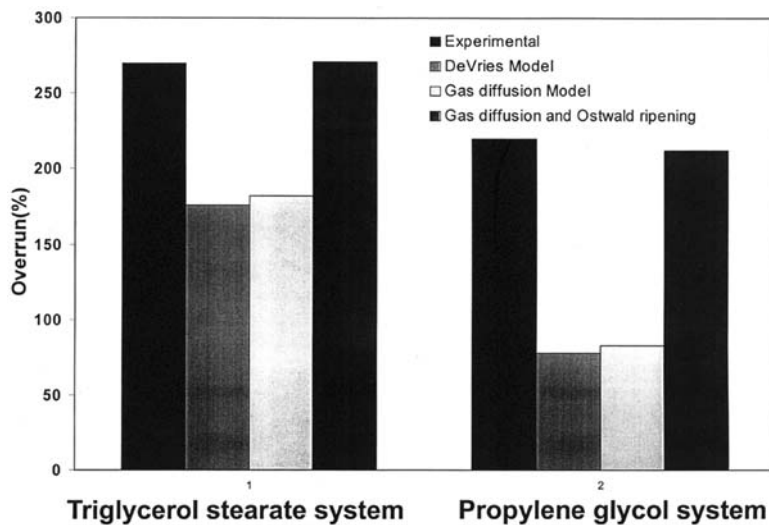


Figure 19 Comparison of experimental and model predicted overruns after 1 week storage at room temperature.

820% to 270% and 1000% to 220% for the triglycerol stearate and propylene glycol systems, respectively). The bubbles would transfer gas among themselves because of the capillary pressure difference. Large bubbles continue to grow at the expense of smaller bubbles. The system approaches a state where the capillary pressure (being inversely proportional to the radius) in most of the bubbles is much lower than it was initially. Thus, the driving force for the transfer of air to the atmosphere decreases with time, resulting in a lower rate of air loss. It must be also be noted that in a system such as the one we studied experimentally, the distance between bubbles is very small, thereby also reducing the diffusion path for Ostwald ripening. Thus, one can expect a reduction in the air loss from the system. We combined the effect of gas diffusion and Ostwald ripening in Eq. (22). The value of $D\phi_\infty\alpha$ is taken as $5 \times 10^{-4} \mu\text{m}^3/\text{s}$ and $8 \times 10^{-4} \mu\text{m}^3/\text{s}$ for the triglycerol stearate and propylene glycol systems, respectively. The estimated value of $D\phi_\infty\alpha$ for the nitrogen-in-water system is $2 \times 10^{-3} \mu\text{m}^3/\text{s}$. The value for $D\phi_\infty\alpha$ for the triglycerol system was chosen in order to match the final overrun. The value of $D\phi_\infty\alpha$ for the propylene glycol system was estimated by using the ratio of the gas-diffusion rate for these two systems [$8 \times 10^{-4} \approx 5 \times 10^{-4}$ (6.8/4.4)]. Figure 19 shows that when the effects of gas diffusion and the Ostwald ripening process are taken into account, the model predictions are in good agreement with the experimental results. Figure 20 depicts the effect of Ostwald ripening on the long-term stability of the aerated mesophase. It can be concluded that the Ostwald ripening process retards the gas-diffusion process by transferring the gas to larger bubbles (the gas-diffusion rate is inversely proportional to the bubble radius).

The bubble size distribution (measured independently) was also used to verify the model predictions. Figure 21 plots the experimental and model predictions of the volume of air distribution among bubbles of different sizes on a cumulative basis for the triglycerol stearate system. The data corresponding to 1 week of aging have been corrected to account for the loss of air from the system. The volume fraction of air in this case refers to the ratio of the volume of air to the initial volume of the system, in order to aid comparison with the initial data. There is a reasonable match between the model and experimental data for the bubble size distribution.

4. Application of Model in Predicting Long-Term Stability of an Aerated Emulsion System

The above model was used to predict the long-term stability of the two different aerated emulsion systems (one containing fatty acid ester as the emulsifier and the other having the sucrose ester as the emulsifier). The bubble size predicted using the model is compared with the experimentally

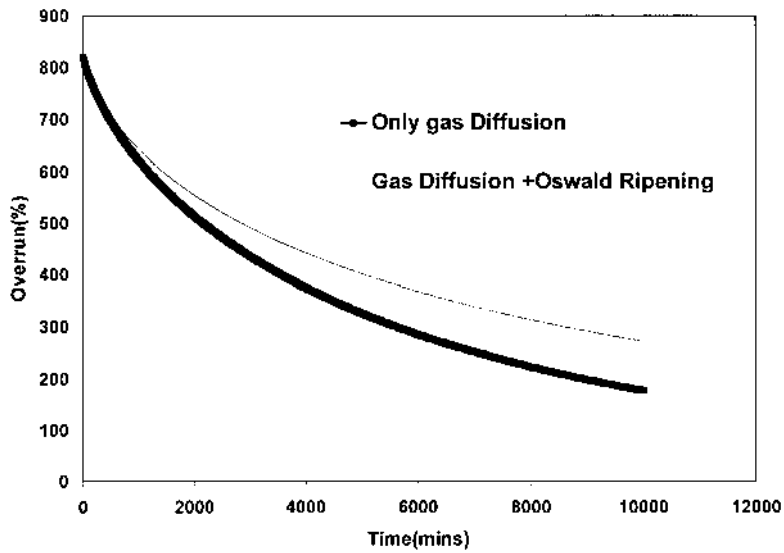


Figure 20 Effect of Ostwald ripening on gas diffusion.

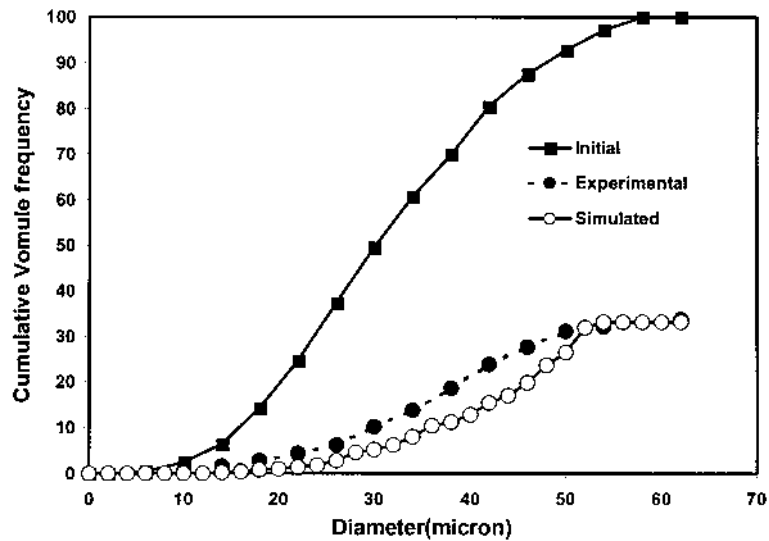


Figure 21 Comparison of experimental bubble size distribution with the model prediction for triglycerol stearate system.

observed bubble size after 1 week. After a period of 1 week, the mean bubble size increased for both emulsion systems. The mean bubble size increased from 41.2 μm to 60 μm in the case of the emulsion containing the fatty acid ester. This confirms our earlier observation about the effect of Ostwald ripening on the bubble size distribution (i.e., larger bubbles grow at the expense of smaller bubbles and this results in a higher mean bubble size). We also obtained good agreement between the experimentally observed bubble size and the model predicted bubble size for both systems (35).

IV. CONCLUSIONS

The study of fat particle structure during the whipping process such as homogenization, cooling, aging, aeration, and whipping revealed that a very poor fat particle structure was produced immediately after homogenization due to the very high temperature of the food emulsions. The fat particle structure improved greatly after cooling. It was observed that the fat particle structure inside low-fat products (5 wt% fat whipped foam and 12 wt% fat whipped foam) does not change with the aging time, whereas the fat particle structure is slightly improved for a high-fat product (20 wt% fat whipped foam), indicating that most of the adsorption of the surfactant and protein on the fat particle surface have been completed before aging. The fat particle structure improved greatly for all the products after whipping, indicating that a well-developed fat particle structure is formed in the bulk phase and stabilizes the foam products.

The foam film rheology and foam film thickness stability produced from fat-in-water emulsions have been investigated using a film rheometer. Several important physical properties, such as equilibrium film tension, dynamic film tension, foam film elasticity, and critical film expansion area, were obtained. A good correlation exists between the stability of foam-based products and the foam film rheological properties. A high foam film elasticity and critical film expansion area and a small value of the initial slope of the curved film tension versus time led to more stable foam-based products.

The stability of aerated emulsions also depends on the air permeability through the foam lamella. Smaller values for foam film permeability yield a higher stability in foam-based food products.

From numerical simulations and experimental studies of the destabilization of the aerated mesophase (overruns were 820% and 1000% for the triglycerol system and the propylene glycol system, respectively), we found that the predominant mechanisms of destabilization are gas diffusion to the atmosphere and Ostwald ripening. The overrun of the system decreases

(from 820% to 270% and from 1000% to 220% for the triglycerol system and propylene glycol system, respectively) with time because of the gas diffusion from the bubbles to the atmosphere. The rate of gas diffusion depends on the permeability of air through the adsorbed layer and mesophase and on the bubble size (driving force is inversely proportional to the bubble size).

Bubbles would transfer gas among themselves due to the capillary pressure difference (the Ostwald ripening phenomenon). Large bubbles continue to grow at the expense of smaller bubbles. Thus, the driving force (being inversely proportional to the radius) for the transfer of air to the atmosphere decreases with time, resulting in a lower rate of air loss. Ostwald ripening also affects the bubble size distribution. Bubbles smaller than the critical size shrink and may eventually disappear. A theoretical model was developed to predict the effects of gas diffusion and Ostwald ripening on the long-term stability of the aerated food products. The gas-diffusion rate was obtained from the shrinking bubble experiments. The model was verified with the experimental results of overrun and good agreement was observed. Model predictions for the bubble size distribution as a function of time are found to be in agreement with the experimentally observed bubble sizes, which were determined by conducting an independent set of experiments.

REFERENCES

1. W. Buchheim, N. M. Barlord, and N. Krog, Relation between microstructure destabilization phenomena and rheological properties of whippable emulsions, *Food Microstruct.* 4, 221–232 (1985).
2. E. C. Needs, Importance of milk proteins to the whippable properties of 38% fat cream, in *Food Colloids, The Proceedings of an International Symposium Organized by the Food Chemistry Group of the Royal Society of Chemistry*, 1988.
3. E. C. Needs and B. E. Brooker, Factors affecting the formation and stabilization of high fat foams, in *Food Polymers, Gels and Colloids, The Proceedings of an International Symposium Organized by the Food Chemistry Group of the Royal Society of Chemistry*, 1990, pp. 227–231.
4. D. F. Darling, Recent advances in the destabilization of dairy emulsions, *J. Dairy Res.* 49, 695–712 (1982).
5. B. E. Brooker, M. Anderson, and A. T. Andrews, The development of structure in whipped cream, *Food Microstruct.* 5, 277–285 (1986).
6. B. E. Brooker, The adsorption of crystalline fat to the air–water interface of whipped cream, *Food Struct.* 9, 223–229 (1990).
7. W. Xu, A. Nikolov, D. T. Wasan, A. Gonsalves, and R. P. Borwankar, Particle structure and stability of colloidal dispersions as probed by Kossel diffraction technique, *J. Colloid Interf. Sci.* 191, 471–481 (1997).

8. E. Dickenson, Food colloids—An overview, *Colloids Surfaces* 42, 191–204 (1989).
9. J. Courthandon, E. Dickinson, and D. G. Dalgleish, Competitive adsorption of β -casein and nonionic surfactants in oil-in-water emulsions, *J. Colloid Interfa. Sci.* 145(2), 391–395 (1991).
10. L. A. Lobo, Stability of emulsions and foams, PhD thesis, Illinois Institute of Technology, Chicago, 1991.
11. E. Dickinson, Interfacial interactions and the stability of oil-in-water emulsions, *Pure Appl. Chem.* 64(11), 1721–1724 (1992).
12. P. Richmond, Food technology and nutrition: Challenges for colloid and interface science, *Pure Appl. Chem.* 64(11), 1751–1755 (1992).
13. J. Chen, E. Dickinson, and G. Iveson, Interfacial interactions, competitive adsorption, and emulsion stability, *Food Struct.* 12, 135–146 (1993).
14. J. M. Soos, K. Koczo, E. Erdos, and D. T. Wasan, An automatic apparatus for measuring interfacial and film tension under static and dynamic conditions, *Rev. Sci. Instrum.* 65(11), 3555–3562 (1994).
15. Y. H. Kim, D. T. Wasan, and P. J. Breen, A study of dynamic interfacial mechanisms for demulsification of water-in-oil emulsions, *Colloids Surfaces* 95, 235–247 (1995).
16. Y. H. Kim, A. D. Nikolov, D. T. Wasan, H. Diaz-Arauzo, and C. S. Shetty, Demulsification of water-in-crude oil emulsions: Effects of film tension, elasticity, diffusive, and interfacial activity of demulsified individual components and their blends, *J. Dispers. Sci. Tech.* 17(1), 33–53 (1996).
17. Y. H. Kim and D. T. Wasan, Effect of demulsifier partitioning on the destabilization of water-in-oil emulsions, *Ind. Eng. Chem. Res.* 35(4), 1141–1149 (1996).
18. Y. H. Kim, K. Koczo, and D. T. Wasan, Dynamic film and interfacial tensions in emulsion and foam systems, *J. Colloid Interfa. Sci.* 187, 29–44 (1997).
19. B. Sood, Study of foam dynamics, texture and stability with application to aerated and foamed products, MS thesis, Illinois Institute of Technology, Chicago, pp. 2.1–2.12.
20. I. M. Lifshitz and V. V. Slyozov, The kinetics of precipitation from supersaturated solid solutions, *J. Phys. Chem. Solids* 19(1/2), 35 (1961).
21. C. Wagner, *Ber. Bunsenges. Phys. Chem.* 65, 581 (1961).
22. A. J. De Vries, Foam Stability Part I, *J. Recueil* 77, 81–91 (1958).
23. A. J. De Vries, Foam Stability Part II, *J. Recueil* 77, 209–223 (1958).
24. H. M. Princen and S. G. Mason, The permeability of soap films to gases. *J. Colloid Sci.* 20, 353–375 (1965).
25. H. M. Princen, J. T. G. Overbeek, and S. G. Mason, The permeability of soap films to gases. II. A simple mechanism to monolayer permeability. *J. Colloid Sci.* 24, 125–130 (1967).
26. A. Prins, Theory and practice of formation and stability of food foams, in *Food Emulsions and Foams* (E. Dickenson, ed.), Special Publication No. 58, The Royal Society of Chemistry, London, 1987, pp. 30–39.
27. A. Arefmanesh and S. G. Advani, *Rheol. Acta* 30, 274 (1991).
28. D. C. Venerus and N. Yala, *Aiche J.* 43, 2948 (1997).

29. D. C. Venerus, N. Yala, and B. Bernstein, *J. Non-Newtonian Fluid Mech.* 75, 55 (1998).
30. D. T. Wasan and A. D. Nikolov, Structure and stability of emulsions, in *Encyclopedic Handbook of Emulsion Technology* (J. Sjoblom, ed.), Marcel Dekker, New York, 2001, pp. 59–70.
31. R. Nagargan, K. Koczo, E. Erods, and D. T. Wasan, Controlled drop tensiometer for measuring dynamic interfacial tension and film tension, *AICE J.* 41(4), 915–923 (1995).
32. M. E. Wijnen and A. Prins, Disproportion in aerosol whipped cream, in *Food Macromolecules and Colloids*, (E. Dickenson and D. Lorient, eds.), Special Publication No. 156, The Royal Society of Chemistry, London, 1995, pp. 309–311.
33. F. Dullien, *Porous Media Fluid Transport and Pore Structure*, Academic Press, New York, 1979.
34. H. D. Goff, The role of chemical emulsifiers and dairy proteins in fat destabilization during the manufacture of ice cream, PhD thesis, Cornell University, Ithaca, NY, 1988.
35. S. Uchil, Structure and stability of imitation dairy cream emulsion, MS thesis, Illinois Institute of Technology, Chicago, 2001.
36. H. W. Yarranton and J. H. Masliyah, Numerical simulation of ripening in emulsions, *J. Colloid Interfa. Sci.* 196, 157–169 (1997).